

Cite this: DOI: 10.1039/c0xx00000x

www.rsc.org/xxxxxx

PAPER

The effect of resonant excitation, pulse duration and intensity on photoelectron imaging of a dianion

Adam S. Chatterley,^{a,b} Daniel A. Horke^{†a} and Jan R. R. Verlet,^{*a}

Received (in XXX, XXX) Xth XXXXXXXXXX 20XX, Accepted Xth XXXXXXXXXX 20XX

DOI: 10.1039/b000000x

The photoelectron imaging of the indigo carmine dianion is used to demonstrate the effects of resonance excitation, pulse duration and pulse intensity on the photoelectron spectra and angular distributions of a dianion. Excitation of the S_1 state leads to an aligned distribution of excited state dianions. The photoelectron angular distribution following subsequent photodetachment within a femtosecond laser pulse is primarily determined by the repulsive Coulomb barrier. Extending the timescale for photodetachment to nanoseconds leads to dramatic changes in both the spectra and angular distributions. These observations are explained in terms of statistical detachment of electrons, either from the monoanion, or from the ground state of the dianion following a number of photon cycles through the $S_1 \leftarrow S_0$ transition. At high intensity, new electron emission channels open up, leading to emission below the repulsive Coulomb barrier. This has been assigned to strong-field induced detachment and the effect of an electric field on the Coulomb barrier is discussed in terms of the photoelectron spectra and angular distributions.

1. Introduction

The angular distribution of photoelectron (PE) emission relative to the polarisation vector of the light field, ϵ , has been extensively studied in neutrals and anions, and has become routine with the advent of charged particle imaging¹ and especially velocity map imaging.² In simple systems the PE angular distribution (PAD) can be well described by the Cooper-Zare formalism³ in which the partial waves and their interference determine the observed PE anisotropy. This works particularly well for atomic photodetachment. In the case of molecular detachment, a complete description of the PAD becomes more challenging, but not impossible, and various aspects of PADs have been recently discussed in excellent reviews.⁴⁻⁸ For both neutrals and anions, the PE experiences a radially attractive potential. For neutrals, this is simply a charge-charge $-1/r$ interaction. For anions, the attractive interaction is much weaker and shorter range, typically dominated by dipole-charge interaction or quadrupole-charge and induced dipole-charge interactions.

The situation is, however, significantly different in multiply-charged anions (MCAs).⁹⁻¹⁴ Take for example a dianion, A^{2-} . Photoemission from A^{2-} leads to the formation of an anion and the PE: $A^{2-} + h\nu \rightarrow A^- + e^-$. At long range, the interaction between A^- and e^- is repulsive. In contrast, at short range, there must be some attraction if the A^{2-} dianion is stable. The net interaction leads to the repulsive Coulomb barrier (RCB) in MCAs, first probed experimentally by the Wang group using PE spectroscopy.¹⁰⁻¹² The tell-tale sign of an RCB in a PE spectrum is a region at low electron kinetic energy (eKE) over which no PE signal can be observed. PE emission is then suddenly allowed at some cut-off, above which the emitted PE has sufficient energy to

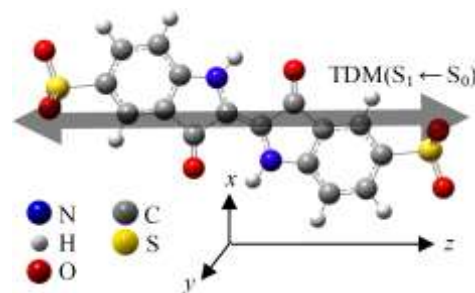


Figure 1. Structure of the doubly-deprotonated indigo carmine dianion. The Cartesian coordinate system is defined along with the transition dipole moment (TDM) for the $S_1 \leftarrow S_0$ transition, which is indicated by the grey arrow. The magnitude of the TDM is $4.55 ea_0$.

surmount the RCB.¹⁰⁻¹² The RCB also has dramatic consequences on the PAD of MCAs in PE imaging experiments.¹⁵⁻²² In contrast to anions and neutrals, the PADs from MCAs have received virtually no theoretical attention. PADs have been interpreted qualitatively using classical arguments based on the shape of the RCB. Although this has provided some satisfactory descriptions of the PADs, the role of quantum interference has not yet been explored.

The shape of the RCB is an important parameter in determining the PAD and the RCB can be highly anisotropic.^{15, 16, 18-23} Indeed, in all but one¹⁹ of the PE imaging studies on MCAs has this clear anisotropy provided direct clues on the influence of the RCB on the PAD. In these systems, the RCB anisotropy can be correlated to the localisation of excess charges, either on SO_3 or CO_2 groups, where the RCB will be maximal.

The present study focuses on the dianion of indigo carmine (InC^{2-}), the structure of which is shown in Fig. 1. Our interest in InC^{2-} stems from its remarkable photostability.²⁴⁻²⁹ Indigo and its derivatives have been used for millennia as decorative dyes due to their vivid blue colour.³⁰ As an example, indigo is the dye that stains denim jeans. We have recently studied the excited state photophysics of InC^{2-} in the gas-phase using time-resolved PE imaging and showed that the mechanism for decay involves an excited state intramolecular proton transfer reaction followed by rapid internal conversion.^{27, 28} Our current focus is on the PE imaging of InC^{2-} .

InC^{2-} presents an interesting system from the viewpoint of PE imaging as it has a highly anisotropic RCB. Previous density functional theory (DFT) calculations showed that the highest occupied orbital (HOMO) of InC^{2-} is the π -system on the chromophore.²⁸ Hence, electron emission from this leaves a positively charged hole in the chromophore, while the two SO_3 groups remain negatively charged and provide a repulsive force on the emitted PE.^{20, 31} Because the RCB is highly anisotropic, one might intuitively anticipate that the PAD will also be highly anisotropic, as long as there exists some correlation between the laboratory and molecular frames of reference. This can either be attained through resonant excitation leading to an aligned sample or by virtue of an anisotropic differential photodetachment cross section. This has been shown previously by the Wang group and our group.^{15-18, 20, 31}

InC^{2-} is related to the system we had previously studied, pyrromethene 556, in the sense that it structurally has an overall similar shape with a central chromophore and two terminal charged groups.^{20, 31} We show that the overall features of InC^{2-} are similar to those of pyrromethene 556, which suggests that it is only the shape of the RCB that determines the PAD (at low eKE).

The present study considers aspects of the PE spectra and PADs following photodetachment from InC^{2-} . Specifically, we consider the effect of pulse duration on the PE spectrum and show that the PAD provides new insight into the emission mechanisms. We also consider, for the first time, the effect of pulse intensity on the PE spectrum and angular distribution and show that the presence of a high electric field can distort the RCB resulting in electron emission below the RCB – analogous to “tunnel ionisation” well-known in high-field physics of neutrals.

2. Experimental

The experiment has been described in detail elsewhere³²⁻³⁵ and only a brief overview is given here. InC^{2-} was generated by electrospray ionisation of a solution of the InC^{2-} disodium salt (Aldrich) in acetonitrile (1 mM). The ions were trapped in a ring-electrode trap and injected into a co-linear Wiley-McLaren time-of-flight mass spectrometer.³⁶ The temporal focus coincides with the laser-interaction point at the centre of a velocity map imaging (VMI) PE spectrometer.² The orthogonal VMI operates in a continuous mode by using a low field arrangement.³⁵

Mass-selected InC^{2-} ions were irradiated with either femtosecond or nanosecond pulses. Femtosecond pulses were derived from a commercial Ti:Sapphire chirped-pulse amplified system. Pulses at 4.7 eV (266 nm) were generated by third harmonic generation using two type I BBO crystals. Pulses at 2.3 eV (538 nm, resonant with the $S_1 \leftarrow S_0$ transition) were generated

using an optical parametric (OP) amplifier, the idler output at 0.75 eV (1640 nm) of which was mixed with residual 1.55 eV (800 nm) in a type I BBO crystal. Pulses at 1.0 eV (1230 nm) used the OP amplifier signal output at that wavelength. Nanosecond pulses were derived from a commercial Nd:YAG (3rd harmonic) pumped OP oscillator. The polarisation of all laser fields, ϵ , was kept parallel to the detector.

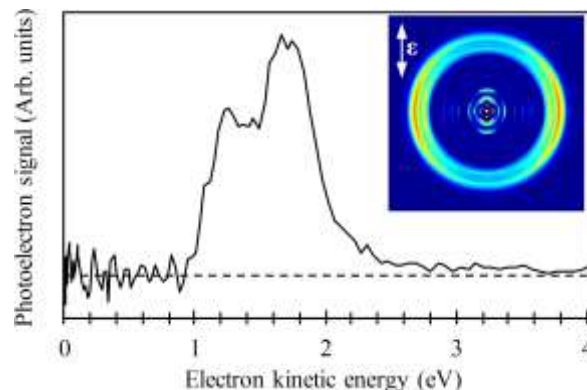


Figure 2. Photoelectron spectrum taken at 4.7 eV at a laser intensity of $I_{UV} \sim 1 \times 10^9 \text{ W cm}^{-2}$. The inset shows the reconstructed image, where ϵ is the laser polarisation axis.

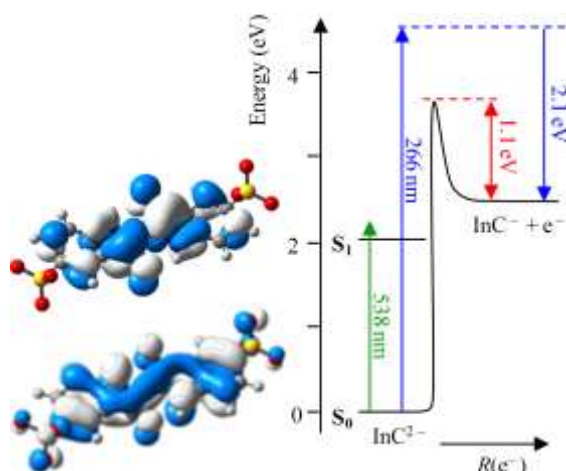
Raw PE images were deconvoluted using the polar ion peeling algorithm.³⁷ Images presented correspond to the central slice through the reconstructed PE cloud; raw images as collected experimentally can be found in the ESI. The resolution of the PE spectrometer was $\sim 5\%$ of the eKE and was calibrated using Γ . Quoted uncertainties in the anisotropy parameters refer to one standard deviation. The absolute accuracy of the anisotropy parameters quoted is on the order of ± 0.1 and arises primarily from variations in alignment and parallelism of ϵ to the detector plane.

3. Results and Discussion

3.1 PE spectrum at 4.7 eV: overview of energetics

The PE spectrum taken at 4.7 eV (266 nm) is shown in Fig. 2 along with its reconstructed PE image inset. As this PE spectrum corresponds to a single photon vertical detachment process, key energetic parameters can be obtained from the spectrum. Specifically, the onset of the PE spectrum is correlated with the outer RCB height, which can be read off to be ~ 1.1 eV. The adiabatic detachment energy, determined from an extrapolation of the steepest onset of signal at high eKE , is about 2.5 eV for InC^{2-} . We had previously also measured an action spectrum of InC^{2-} by monitoring only the electron loss channel and this indicated a broad absorption with a maximum at 2.2 eV (560 nm).²⁸ An overview of the energy level diagram of InC^{2-} is shown in Fig. 3 and this compares well with previous DFT calculations computed with the Gaussian09 package³⁸ and using the B3LYP functional³⁹ with a 6-311++G** basis set. InC^{2-} is a closed shell molecule with a singlet ground state, S_0 . The HOMO of InC^{2-} is the π -system on the chromophore (see Fig. 3), while the SO_3^- orbitals are calculated to lie ~ 0.1 eV below this. The observed PE spectrum at 4.7 eV may therefore contain detachment from either the HOMO or the SO_3^- groups. This may be reflected by the bimodal distribution observed in the PE spectrum. The absorption

around 2.2 eV corresponds to the promotion of an electron from the HOMO to the lowest unoccupied orbital (LUMO), which is also shown in Fig. 3.



5 Figure 3. Energy level diagram for the indigo carmine dianion, showing the relevant states of the system and excitation schemes.

Also shown are the highest occupied and lowest unoccupied molecular orbitals.

The PE image at 4.7 eV (266 nm) is anisotropic with an anisotropy parameter of $\beta_2 = -0.33 \pm 0.03$. For neutrals or monoanions, the PAD is determined by the weight of outgoing partial waves as well as the interference between these.⁴ In MCAs, this inherent anisotropy appears to be trumped by the repulsive long-range Coulombic interaction of the remaining negative charges on the PE. In non-resonant single-photon PE spectra, such effects are only observable if there is also anisotropy in the photodetachment differential cross-section.²⁰ This appears to be the case for InC^{2-} photodetached at 4.7 eV and suggests that the differential cross-section peaks along the z-axis of InC^{2-} (defined in Fig. 1).

3.2 Effect of resonance-enhancement on PE images

The effect of the RCB on the outgoing PE can be more precisely shown by alignment of the sample prior to photodetachment.²⁰ Here, this is achieved by photo-excitation of InC^{2-} from the S_0 to the bright S_1 state. The transition dipole moment calculated using time-dependent DFT and the same level of theory as described in the previous section is indicated in Fig. 1. Fig. 4(a) shows the PE spectrum of InC^{2-} taken at 2.3 eV (538 nm), with a laser intensity below the onset of strong field effects ($I_{fs} \sim 1 \times 10^{10} \text{ W cm}^{-2}$). The overall shape of the PE spectrum is consistent with that observed at 4.7 eV, assuming the absorption of 2-photons (a single photon at 2.3 eV is below the adiabatic detachment energy of InC^{2-}). Specifically, the RCB cut-off at low eKE is clearly visible and at high eKE , the PE spectrum is consistent with the absorption of 2 photons. Given that 2.3 eV is resonant with the $S_1 \leftarrow S_0$ transition, this 2-photon process is resonantly enhanced. Excitation of the S_1 will lead to an aligned sample of excited InC^{2-} molecules with a $\cos^2\theta$ distribution, where θ is the angle between the transition dipole moment between S_0 and S_1 (see Fig. 1) and the laser polarisation vector, ϵ . The second photon, which is absorbed during the 100 fs laser pulse, then projects the S_1 state onto the $\text{InC}^- + e^-$ continuum and the resulting PE will leave

under the influence of the RCB.

In the present case, the RCB is qualitatively described by the fact that the SO_3 groups remain negatively charged while there is a positive hole on the π -system of the chromophore. The reconstructed PE image following 2-photon detachment at 2.3 eV is shown inset in Fig. 4(a). The image is highly anisotropic and is quantified by $\beta_2 = -0.89 \pm 0.05$ and $\beta_4 = 0.11 \pm 0.05$. This is significantly more anisotropic than the single photon 4.7 eV PE image, although the final energy is approximately the same. The increased anisotropy can be qualitatively accounted for by the

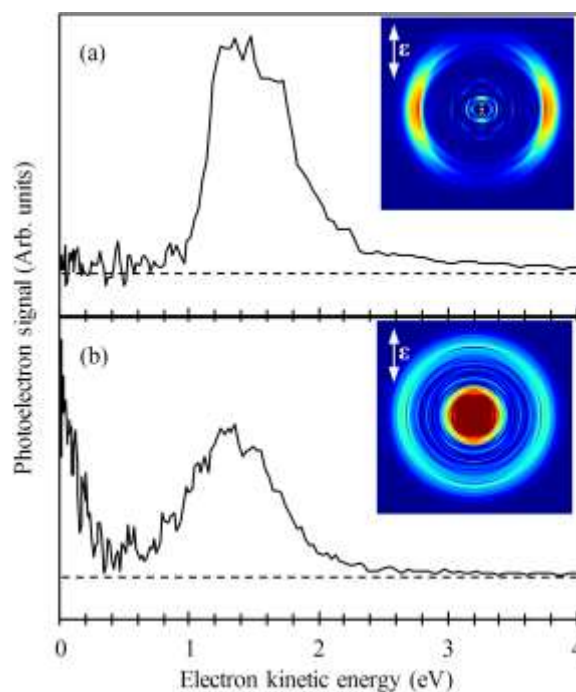


Figure 4. Photoelectron spectrum taken at 2.3 eV with femtosecond (a) and nanosecond (b) pulses. The laser intensities were $I_{fs} \sim 1 \times 10^{10} \text{ W cm}^{-2}$ and $I_{ns} \sim 7 \times 10^6 \text{ W cm}^{-2}$, respectively. The insets show the reconstructed images, where ϵ is the laser polarisation axis.

influence of the RCB on the outgoing PE. Detachment with the second photon occurs from an aligned ensemble of S_1 excited InC^{2-} molecules. Along ϵ , the SO_3^- groups pose very large Coulomb barriers and the PE is prevented from departing along the z-direction (Fig. 1). Instead, the lowest RCB is the perpendicular plane. Hence, the photoemission is initially directional within this plane. Additionally, at long-range the repulsion of the PE with the SO_3^- groups will further influence the outgoing PE. The resultant PAD is therefore expected to strongly peak in the direction perpendicular to ϵ and this is observed experimentally in Fig. 4(a).

The observed PE anisotropy is similar to that previously recorded for pyromethene 556, which has a broadly similar structure and also has a transition dipole moment for excitation along the axis containing SO_3^- groups.^{20, 31}

The 2-photon spectrum in Fig. 4(a) almost exclusively arises from detachment of an electron in the HOMO due to resonance-enhancement. The shape of this spectrum differs from the PE spectrum taken at 4.7 eV (Fig. 2), which showed an additional peak at $eKE \sim 1.7$ eV. The presence of this peak may reflect

detachment from the SO_3^- groups as suggested earlier.

3.3 Effect of pulse duration on PE anisotropy: nanosecond vs. femtosecond

In Fig. 4(b), we show a PE spectrum taken at 2.30 eV (538 nm) using a nanosecond laser, which can be directly compared to the femtosecond PE spectrum in Fig. 4(a). The insets show the corresponding reconstructed images. There are striking differences between these two spectra. Firstly, in the nanosecond spectrum there is no longer a clear RCB cut-off around $eKE = 1.1$ eV. Secondly, there is a new feature peaking at $eKE = 0$ eV, which is below the RCB cut-off. The difference between these two spectra indicates that the extended pulse duration leads to new processes.

In our previous study on InC^{2-} , we showed that the S_1 state is short lived, with a lifetime of 1.2 ps.²⁸ Hence, the S_1 lifetime is an order of magnitude longer than our femtosecond pulses, but at least 3 orders of magnitude shorter than the nanosecond pulses. The consequence of this is that multiple photons can be absorbed using the same $S_1 \leftarrow S_0$ transition, leading to large amounts of energy into the internal modes of InC^{2-} (2.30 eV per photon cycle).

The PE feature peaking at $eKE = 0$ eV probably arises from the monoanion, InC^- , which may be formed by fragmentation after the deposition of a large amount of internal energy following one, two, or more photon-cycles. The low- eKE feature can be then assigned to statistical electron emission from InC^- . In such a scenario, one would expect the PE spectrum to decay exponentially. This is consistent with the observed PE spectrum in Fig. 4(b). We note that similar emission has been observed in dianions studied by our group³¹ and the Wang group¹⁸ and have been interpreted in a broadly similar manner.

The feature that was assigned to 2-photon detachment in the femtosecond spectrum also appears very different in the nanosecond spectrum. Moreover, the observed PADs for these features are very different: $\beta_2 = -0.12 \pm 0.04$ for the nanosecond PE spectrum while it is $\beta_2 = -0.89$ ($\beta_4 = 0.11$) for the femtosecond spectrum. These stark differences imply that the mechanism for detachment may not be the same in the two cases.

We have recently presented an explanation for such observed photodetachment changes with pulse length³¹ and invoke a similar argument here. Briefly, excitation to the S_1 state results in rapid internal conversion, dumping 2.30 eV into the internal modes of InC^{2-} . This energy is redistributed by internal vibrational redistribution (IVR) before a second photon is absorbed. The total energy after the absorption of the second photon is above the adiabatic binding energy plus the RCB (~ 3.6 eV). However, we have previously argued that an increase in internal energy is correlated with a roughly similar increase in the inner RCB height (as viewed by the InC^{2-}) because the initial states correlate adiabatically with the final product states.^{19, 31} Hence, direct detachment is inhibited by the RCB. In any case, the $S_1 \leftarrow S_0$ cross-section is likely to be much larger than direct detachment. Therefore, the second photon excites the $S_1 \leftarrow S_0$ transition again. Although the shapes of the relevant RCB surfaces may be different for this second cycle, the S_1 state will still be bound by these RCB surfaces. Consequently, the electron cannot simply be emitted. It can, however, detach if sufficient time is available to statistically sample lower-lying RCB surfaces

over which the electron may be emitted.³¹

In our study on pyromethene 556, the internal conversion time was determined to be >100 ps.³¹ In that case, IVR on the S_1 state would be almost complete and modes leading to electron emission over a sufficiently low RCB could be statistically sampled from the S_1 or the S_0 states, but we could not distinguish from which.³¹ In the present case, the lifetime of the S_1 is only 1.2 ps and so there is insufficient time for extensive IVR on the S_1 excited state. Hence, the statistical electron emission is likely to be exclusively from the S_0 ground state. This picture is supported by the PADs.

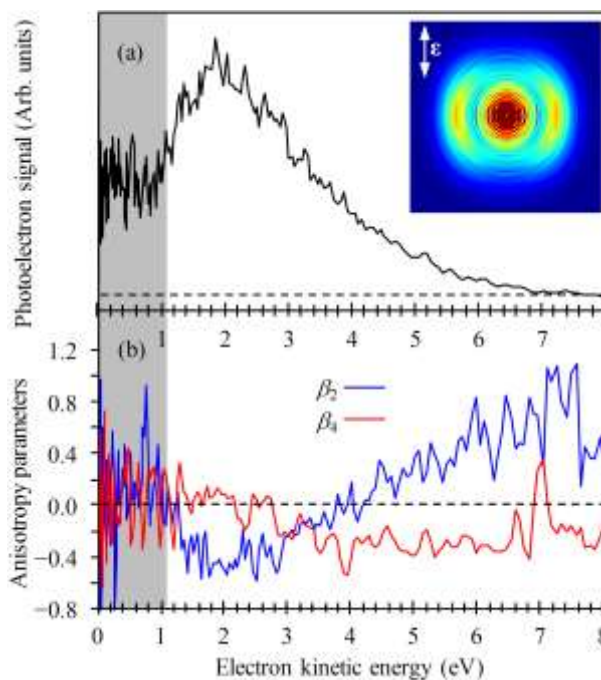


Figure 5. (a) Photoelectron spectrum taken at 1.0 eV with a femtosecond pulse of intensity, $I \sim 7 \times 10^{12} \text{ W cm}^{-2}$. The inset shows the reconstructed image, where ϵ is the laser polarisation axis. (b) Photoelectron anisotropy parameters, β_2 and β_4 for the spectrum in (a).

The PAD for the PE feature between $1 < eKE < 2$ eV in the nanosecond experiment (inset, Fig. 4(b)) reveals an almost isotropic distribution ($\beta_2 = -0.12 \pm 0.04$). If emission was occurring from the S_1 state within its lifetime of 1.2 ps, then the PAD would be anisotropic because of the strongly directional transition dipole moment of the $S_1 \leftarrow S_0$ transition and the fact that the rotational dephasing lifetime is longer than the S_1 lifetime.²⁰ Instead, if emission was occurring from the S_0 ground state with 4.6 eV of internal energy, then this would proceed purely statistically over an extended timescale. Correspondingly, there would be no correlation between the molecular frame and laboratory frame and the observed PAD would therefore be isotropic. The observed PAD for this feature is predominantly isotropic, with a small component perpendicular to ϵ . Hence, it appears that most of the electron loss is occurring from the S_0 state.

3.4 High intensity effects: Observation of strong-field ionisation

In Fig 5(a), we show a PE spectrum taken at 1.0 eV (1230 nm)

with the femtosecond laser beam focussed in the interaction region. We estimate an intensity of $\sim 7 \times 10^{12} \text{ W cm}^{-2}$. The inset shows the reconstructed PE image and in Fig 5(b), PE anisotropy parameters are shown as a function of eKE . We have only included β_2 and β_4 , although the image was fit to include all parameters up to and including β_8 . These have been omitted because they are essentially zero. Note that 1.0 eV is not resonant with any transitions in the system, although 2 photons will be resonant with the red edge of the $S_1 \leftarrow S_0$ transition.

The PE spectrum has a very different appearance to that discussed previously. The most striking difference is that there is a significant and constant PE signal *below* the RCB cut-off. These electrons are emitted almost isotropically from the system. For $eKE > 1.1$ eV, there appears to be some structure in the PE spectrum. The increase in PE signal at the RCB cut-off is accompanied by a change in PE anisotropy. At higher eKE , this anisotropy changes, with the higher order β_4 also contributing.

The observed increase at $eKE = 1.1$ eV suggests that multiphoton detachment is possible through a $2 + n$ resonance-enhanced scheme, where $n \geq 2$. The PE spectrum extends to $eKE \sim 7$ eV, implying the absorption of up to 10 photons. This multiphoton absorption process should not, however, allow for PE emission below the RCB. Between $1.1 < eKE < 1.8$ eV, β_2 steadily decreases from close to zero to -0.4 . It then remains at -0.4 between $1.8 < eKE < 2.8$ eV. Beyond 2.8 eV, there is a steady increase in β_2 , rising from -0.4 to $+0.5$ at $eKE \sim 6$ eV. At the same time, β_4 over this spectral region is approximately -0.3 . Higher order anisotropy parameters are approximately zero. The broad feature between $1.1 < eKE < 2.8$ eV has the overall appearance of multi-photon absorption and the negative anisotropy is consistent with that observed using 2-photon resonance enhanced detachment (Fig. 4(a)). We had anticipated that the alignment may be stronger rather than weaker because of the absorption of multiple photons, but it should be noted that this feature is clearly convoluted with the electron emission at low eKE . Hence, it is very difficult to comment further within the scope of this article.

The key observation here is the fact that PE signal is observed *below* the RCB. This signal arises only at high laser intensity and, under such conditions, we have in fact observed similar PE emission in many of the dianions studied in our lab and at several wavelengths. Hence, this observation is a more general feature of dianions (or indeed MCAs) and depends only on the electric field strength. In neutrals, strong-field ionisation is a well-known phenomenon and has found great application in, for example, high-harmonic generation⁴⁰ and attosecond science,⁴¹ where the $-1/r$ Coulomb potential is pulled down sufficiently far in the electric field of the laser that the electron can tunnel out into the continuum. A similar mechanism is likely to be operative in InC^{2-} , but at significantly lower field strengths.

We can crudely approximate the RCB for InC^{2-} as being composed of two negative and one positive point-charges, plus an electron whose position is a variable (see Fig. 6(a)). The negative charges (defined here as the centre of the triangle formed by the O atoms on each SO_3 determined by our DFT calculations) are separated by 15.5 \AA . The resultant RCB is simply the Coulomb interaction of the electron with the two negative charges and the hole. In Fig. 6(c), the RCB is calculated along the x (or y)

direction. The saddle point in the RCB is in the xy plane and the lowest point along of the RCB in this plane is calculated as 0.84 eV. This is somewhat lower than that observed (1.1 eV), probably because of the delocalised nature of the electrons and, in particular, the hole. Also shown in Fig. 6(c) is the RCB in which dc electric fields in the x direction have been added. For a field strength of $E = 9.9 \times 10^8 \text{ V m}^{-1}$ ($I = 1.3 \times 10^{11} \text{ W cm}^{-2}$), corresponding to a 100 μJ , 100 fs pulse focussed to a 1 mm diameter spot size, the RCB is reduced to 0.01 eV in the $+x$ direction. Hence, despite these relatively mild focussing

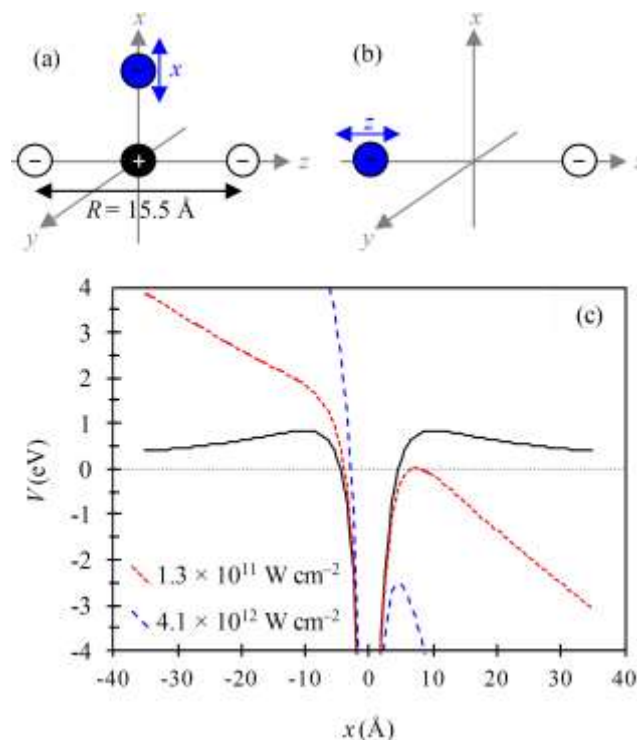


Figure 6. Schematic of point-charge distributions used to estimate the repulsive Coulomb barrier for the molecular system in which an electron is detached from (a) the chromophore and (b) the SO_3^- group. The Coulomb field experienced for (a) is calculated (black) along with the inclusion of an electric field corresponding to the laser field intensities as indicated.

conditions, the RCB has been completely suppressed. To cause direct field ionisation from the S_0 state requires $E = 5.6 \times 10^9 \text{ V m}^{-1}$, which corresponds to an intensity of $4.1 \times 10^{12} \text{ W cm}^{-2}$. It should be noted that the experimental RCB is measured to be larger than that calculated and so the intensity required to cause strong-field ionisation is likely to be somewhat larger.

Under our experimental conditions, we estimate that the intensity in the interaction region is $\sim 7 \times 10^{12} \text{ W cm}^{-2}$. This is close to the intensity required to achieve strong-field ionisation and/or tunnel ionisation from the S_0 ground state. Hence, it is not unreasonable to assign the electron emission at $eKE < 1.1$ eV to such processes. In strong-field physics, the prominence of tunnel ionisation relative to multiphoton ionisation can be crudely determined by the Keldysh parameter, $\gamma = (I_p / 2U_p)^{1/2}$, where I_p is the ionisation potential and U_p the pondermotive potential.^{42, 43} If $\gamma < 1$, then tunnelling dominates; if $\gamma > 1$, multiphoton ionisation dominates. Although the Keldysh parameter is based on a $-1/r$ potential, we can still estimate γ by replacing I_p with the adiabatic

binding energy plus the RCB. From Fig. 2, this was estimated to be 3.6 eV, so that $\gamma \sim 1.4$. Hence, both tunnel ionisation and multiphoton ionisation are expected to occur.

Fig. 5 shows that electron emission due to strong-field ionisation is isotropic. Considering the above picture, this observation is not expected because the laser field is polarised. In the scenario outlined in Fig. 6(a), the RCB is much higher along the z -direction and it is unlikely that field ionisation from the HOMO will occur along this direction. Hence, only InC^{2-} molecules that are distributed perpendicular to ϵ will be expected to strong-field ionise. This should result in a clear anisotropy of the emitted electrons along the ϵ direction (*i.e.* $\beta_2 > 0$). Experimentally, the low eKE signal is isotropic. This discrepancy may be attributed to (i) resonant excitation of the S_1 state from which strong-field ionisation then occurs or (ii) field ionisation of the SO_3^- groups.

The former possibility would lead to a more isotropic distribution because the 2-photon excitation step will lead to some alignment of the z -axis of the S_1 excited InC^{2-} molecules along ϵ . The same laser field will cause strong-field ionisation, but the emission from the aligned sample can only occur if ϵ was perpendicular to the z -axis. However, both the photo-excitation and field ionisation steps will have some distribution of alignment angles, θ . Therefore, strong-field ionisation can still occur but it will be roughly isotropic. For example, the product between a $\cos^2\theta$ and a $\sin^2\theta$ distribution will lead to electron emission peaking at $\theta = \pi/4$.

Strong-field ionisation from SO_3^- is also likely and this is shown schematically in Fig. 6(b). Based on simple electrostatic arguments, the Coulomb interaction between the two SO_3^- groups is approximately 0.9 eV. This will lead to an RCB that is similar to that in the xy -plane for detachment from the HOMO. This RCB is also sensitive to the electric field and the SO_3^- may thus also be susceptible to strong-field ionisation in much the same way as the HOMO. Field ionisation from SO_3^- , however, can occur for any relative alignment and thus may be expected to lead to a predominantly isotropic PAD as observed. Tunnel ionisation may also occur, but this is expected to lead to a PAD directed predominantly along the z -direction. The energy of the molecular orbitals of the SO_3^- groups are calculated to be sufficiently close to the HOMO so that these processes are feasible. Unfortunately, the observed isotropic PAD does not reveal which of the above mechanisms is dominant or operative.

Finally, it should be noted that the strong-field dynamics discussed here are based on the quasi-static model.⁴⁰ One of the core assumptions of this is that the electron dynamics can adiabatically follow the laser field. In the present case, this may not be true as has been observed in large polyatomic neutral molecules,^{44, 45} and non-adiabatic multi-electron dynamics can lead to electron emission. Such emission may also be contributing to the observed PE spectrum.

Our data present the first direct measurement of strong-field ionisation of an MCA in a laser field. To fully understand the complex dynamics due to strong-field ionisation and tunnel ionisation, more experiments are clearly required. Specifically, the use of two-colour experiments and strong-field ionisation with far off-resonance fields should prove informative. Nevertheless, our observations carry some important implications

and opportunities for experiments on MCAs. The key observation is that, even at rather modest peak intensities, the RCB can be dramatically affected by the electric field. This will be even more dramatic for larger systems in which the separation between charge sites is larger. Femtosecond experiments will be most sensitive to these effects, but focussed nanosecond pulses can also have noticeable effects. In the model presented in Fig. 6(a), a 10 mJ, 5 ns pulse focussed down to 0.1 mm spot lowers the RCB by more than 50%. In terms of opportunities, the PADs following field ionisation are expected to show clear signs of the shape of the RCB and hence, strong-field ionisation may be used as a probe for the crude structure of a molecular system.

Conclusions

The PE spectroscopy and imaging of the InC^{2-} dianion has been presented. The focus was on the effect of resonance-enhancement, pulse duration and peak intensity on the PE spectra and angular distributions. The main findings can be summarised as follows:

(1) Photodetachment from an aligned ensemble of InC^{2-} leads to a PAD that can be qualitatively described by considering the shape of the RCB. This is demonstrated here by resonant excitation of the chromophore, which has a well-defined transition dipole moment (Fig. 1), using a polarised femtosecond pulse. This is consistent with previous observations^{20, 31} and suggests that the RCB has a determining impact on the PAD of the outgoing PE. In order to correlate the observed PAD to the RCB shape, however, the correlation between molecular and laboratory frame must be established.²⁰ [The experimental PAD may also be used to determine the anisotropy of the RCB. This would require careful simulation of the outgoing electron which will likely require a full quantum description to account for possible interference and diffraction effects.](#)

(2) Nanosecond excitation via the $S_1 \leftarrow S_0$ transition leads to dramatic changes in both the PE spectra and PADs. This can be explained in terms of a multiple-photon cycling scheme: excitation to S_1 is followed by rapid (1.2 ps) internal conversion; a subsequent photon can then be absorbed via the $S_1 \leftarrow S_0$ transition again followed by internal conversion. The resultant internal energy is sufficient to cause either: dissociation followed by electron loss from the anion, InC^- , leading to a feature peaking around $eKE = 0$ eV; or statistical electron loss from the dianion over the lowest RCB surfaces. As these processes are slow relative to the rotational dynamics of the system, the resultant PADs for these features is approximately isotropic.

(3) At high laser intensity, photoelectrons are emitted below the RCB, producing a constant signal which is roughly isotropic. This emission can be accounted for by considering the effect of the electric field of the laser on the RCB surface. It shows that strong-field ionisation can occur, even from the S_0 state, under the modest experimental conditions. The PADs for various scenarios are considered and this suggests that, for InC^{2-} , strong-field ionisation from the central chromophore, from the SO_3^- groups, and from the S_1 excited state may be operative.

Acknowledgements

We are grateful to the: EPSRC, for funding (EP/D073472/1) and

the loan of the Nd:YAG system through the laser loan pool; the Leverhulme Trust for funding (ASC and JRRV); and the European Research Council for a Starting Grant (JRRV).

Notes and references

^a Department of Chemistry, University of Durham, Durham DH1 3LE, United Kingdom.

^b Department of Chemistry, University of Warwick, Coventry CV4 7AL, United Kingdom.

[†] Current address: Center for Free-Electron Laser Science, DESY,

Notkestr. 85, 22607 Hamburg, Germany

* Correspondence: j.r.r.verlet@durham.ac.uk

1. D. W. Chandler and P. L. Houston, *J. Chem. Phys.*, 1987, **87**, 1445-1447.
2. A. Eppink and D. H. Parker, *Rev. Sci. Instrum.*, 1997, **68**, 3477-3484.
3. J. Cooper and R. N. Zare, *J. Chem. Phys.*, 1968, **48**, 942-943.
4. K. L. Reid, *Annu. Rev. Phys. Chem.*, 2003, **54**, 397-424.
5. A. Sanov and R. Mabbs, *Int. Rev. Phys. Chem.*, 2008, **27**, 53-85.
6. R. Mabbs, E. R. Grumbling, K. Pichugin and A. Sanov, *Chem. Soc. Rev.*, 2009, **38**, 2169-2177.
7. K. L. Reid, *Mol. Phys.*, 2012, **110**, 131-147.
8. A. Stolow, A. E. Bragg and D. M. Neumark, *Chem. Rev.*, 2004, **104**, 1719-1757.
9. M. K. Scheller, R. N. Compton and L. S. Cederbaum, *Science*, 1995, **270**, 1160-1166.
10. L. S. Wang, C. F. Ding, X. B. Wang, J. B. Nicholas and B. Nicholas, *Phys. Rev. Lett.*, 1998, **81**, 2667-2670.
11. X. B. Wang, C. F. Ding and L. S. Wang, *Phys. Rev. Lett.*, 1998, **81**, 3351-3354.
12. L. S. Wang and X. B. Wang, *J. Phys. Chem. A*, 2000, **104**, 1978-1990.
13. J. Simons, *J. Phys. Chem. A*, 2008, **112**, 6401-6511.
14. A. Dreuw and L. S. Cederbaum, *Chem. Rev.*, 2002, **102**, 181-200.
15. X.-P. Xing, X.-B. Wang and L.-S. Wang, *J. Phys. Chem. A*, 2009, **113**, 945-948.
16. X.-P. Xing, X.-B. Wang and L.-S. Wang, *J. Chem. Phys.*, 2009, **130**, 074301
17. C.-G. Ning, P. D. Dau and L.-S. Wang, *Phys. Rev. Lett.*, 2010, **105**, 263001.
18. X.-P. Xing, X.-B. Wang and L.-S. Wang, *J. Phys. Chem. A*, 2010, **114**, 4524-4530.
19. D. A. Horke, A. S. Chatterley and J. R. R. Verlet, *Phys. Rev. Lett.*, 2012, **108**, 083003.
20. D. A. Horke, A. S. Chatterley and J. R. R. Verlet, *J. Phys. Chem. Lett.*, 2012, **3**, 834-838.
21. D. Phuong Diem, H.-T. Liu, J.-P. Yang, M.-O. Winghart, T. J. A. Wolf, A.-N. Unterreiner, P. Weis, Y.-R. Miao, C.-G. Ning, M. M. Kappes and L.-S. Wang, *Physical Review A*, 2012, **85**, 064503.
22. M.-O. Winghart, J.-P. Yang, M. Kuehn, A.-N. Unterreiner, T. J. A. Wolf, P. D. Dau, H.-T. Liu, D.-L. Huang, W. Klopper, L.-S. Wang and M. M. Kappes, *Phys. Chem. Chem. Phys.*, 2013, **15**, 6726-6736.
23. J. B. Williams, C. S. Trevisan, M. S. Schoeffler, T. Jahnke, I. Bocharova, H. Kim, B. Ulrich, R. Wallauer, F. Sturm, T. N. Rescigno, A. Belkacem, R. Doerner, T. Weber, C. W. McCurdy and A. L. Landers, *Phys. Rev. Lett.*, 2012, **108**, 233002.
24. M. N. R. Ashfold, B. Cronin, A. L. Devine, R. N. Dixon and M. G. D. Nix, *Science*, 2006, **312**, 1637-1640.
25. I. Iwakura, A. Yabushita and T. Kobayashi, *Chem. Phys. Lett.*, 2010, **484**, 354-357.
26. I. Iwakura, A. Yabushita and T. Kobayashi, *Bull. Chem. Soc. Jpn.*, 2011, **84**, 164-171.
27. S. Yamazaki, A. L. Sobolewski and W. Domcke, *Phys. Chem. Chem. Phys.*, 2011, **13**, 1618-1628.
28. A. S. Chatterley, D. A. Horke and J. R. R. Verlet, *Phys. Chem. Chem. Phys.*, 2012, **14**, 16155-16161.
29. G. Cui and W. Thiel, *Phys. Chem. Chem. Phys.*, 2012, **14**, 12378-12384.
30. E. S. B. Ferreira, A. N. Hulme, H. McNab and A. Quye, *Chem. Soc. Rev.*, 2004, **33**, 329-336.
31. D. A. Horke, A. S. Chatterley and J. R. R. Verlet, *J. Chem. Phys.*, 2013, **139**, 084302.
32. J. Lecointre, G. M. Roberts, D. A. Horke and J. R. R. Verlet, *J. Phys. Chem. A*, 2010, **114**, 11216-11224.
33. D. A. Horke, G. M. Roberts and J. R. R. Verlet, *J. Phys. Chem. A*, 2011, **115**, 8369-8374.
34. D. A. Horke and J. R. R. Verlet, *Phys. Chem. Chem. Phys.*, 2011, **13**, 19546-19552.
35. D. A. Horke, G. M. Roberts, J. Lecointre and J. R. R. Verlet, *Rev. Sci. Instrum.*, 2012, **83**, 063101.
36. W. C. Wiley and I. H. McLaren, *Rev. Sci. Instrum.*, 1955, **26**, 1150-1157.
37. G. M. Roberts, J. L. Nixon, J. Lecointre, E. Wrede and J. R. R. Verlet, *Rev. Sci. Instrum.*, 2009, **80**, 053104.
38. M. J. Frisch, G. W. Trucks, H. B. Schlegel, G. E. Scuseria, M. A. Robb, J. R. Cheeseman, G. Scalmani, V. Barone, B. Mennucci, G. A. Petersson, H. Nakatsuji, M. Caricato, X. Li, H. P. Hratchian, A. F. Izmaylov, J. Bloino, G. Zheng, J. L. Sonnenberg, M. Hada, M. Ehara, K. Toyota, R. Fukuda, J. Hasegawa, M. Ishida, T. Nakajima, Y. Honda, O. Kitao, H. Nakai, T. Vreven, J. A. Montgomery, J. E. Peralta, F. Ogliaro, M. Bearpark, J. J. Heyd, E. Brothers, K. N. Kudin, V. N. Staroverov, R. Kobayashi, J. Normand, K. Raghavachari, A. Rendell, J. C. Burant, S. S. Iyengar, J. Tomasi, M. Cossi, N. Rega, J. M. Millam, M. Klene, J. E. Knox, J. B. Cross, V. Bakken, C. Adamo, J. Jaramillo, R. Gomperts, R. E. Stratmann, O. Yazyev, A. J. Austin, R. Cammi, C. Pomelli, J. W. Ochterski, R. L. Martin, K. Morokuma, V. G. Zakrzewski, G. A. Voth, P. Salvador, J. J. Dannenberg, S. Dapprich, A. D. Daniels, Farkas, J. B. Foresman, J. V. Ortiz, J. Cioslowski and D. J. Fox, *Gaussian 09, Revision A.02*, Wallingford CT, 2009.
39. P. J. Stephens, F. J. Devlin, C. F. Chabalowski and M. J. Frisch, *J. Phys. Chem.*, 1994, **98**, 11623-11627.
40. P. B. Corkum, *Phys. Rev. Lett.*, 1993, **71**, 1994-1997.
41. F. Krausz and M. Ivanov, *Rev. Mod. Phys.*, 2009, **81**, 163-234.
42. L. V. Keldysh, *Sov. Phys. JETP*, 1965, **20**, 1307-1314.
43. T. Brabec and F. Krausz, *Rev. Mod. Phys.*, 2000, **72**, 545-591.
44. M. Lezius, V. Blanchet, D. M. Rayner, D. M. Villeneuve, A. Stolow and M. Y. Ivanov, *Phys. Rev. Lett.*, 2001, **86**, 51-54.
45. M. Lezius, V. Blanchet, M. Y. Ivanov and A. Stolow, *J. Chem. Phys.*, 2002, **117**, 1575-1588.